THE JOURNAL OF PHYSICAL CHEMISTRY B

ARTICLE

pubs.acs.org/JPCB

The Electronically Excited States of LH2 Complexes from *Rhodopseudomonas acidophila* Strain 10050 Studied by Time-Resolved Spectroscopy and Dynamic Monte Carlo Simulations. I. Isolated, Non-Interacting LH2 Complexes

Tobias J. Pflock,[†] Silke Oellerich,[†] June Southall,[‡] Richard J. Cogdell,[‡] G. Matthias Ullmann,[§] and Jürgen Köhler[†,*]

[†]Experimental Physics IV and BIMF, University of Bayreuth, D-95440 Bayreuth, Germany

[‡]Institute of Molecular, Cell and Systems Biology, College of Medical Veterinary and Life Sciences, Biomedical Research Building, University of Glasgow, Glasgow G12 8QQ, Scotland, U.K.

[§]Computational Biochemistry/Bioinformatics, University of Bayreuth, D-95440 Bayreuth

Supporting Information

ABSTRACT: We have employed time-resolved spectroscopy on the picosecond time scale in combination with dynamic Monte Carlo simulations to investigate the photophysical properties of light-harvesting 2 (LH2) complexes from the purple photosynthetic bacterium *Rhodopseudomonas acidophila*. The variations of the fluorescence transients were studied as a function of the excitation fluence, the repetition rate of the excitation and the sample preparation conditions. Here we present the results obtained on detergent solubilized LH2 complexes, i.e., avoiding intercomplex interactions, and show that a simple four-state model is sufficient to grasp the experimental observations quantitatively without the need for any free parameters. This approach allows us to obtain a quantitative measure for the singlet−triplet annihilation rate in isolated, noninteracting LH2 complexes.

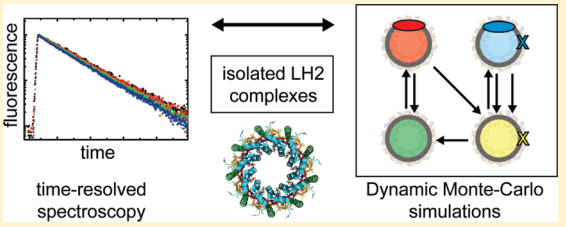

INTRODUCTION

The essential feature of photosynthesis is the conversion of light energy into chemical (redox) energy that can be used as the driving force for subsequent metabolic reactions. However, exploitation of sunlight as a source for energy requires an efficient light-harvesting apparatus for collecting as many photons as possible. This is accomplished by a network of pigment−protein complexes that serve as antennas, i.e., proteins that capture photons and transfer the excitation energy with high efficiency to a specialized pigment−protein complex, the photosynthetic reaction center (RC), that acts as the key transducer.[1]

Purple photosynthetic bacteria have evolved an elegant system of modular units that make up the light-harvesting apparatus.[2,3] Most species have two main types of complexes, the core complex, RC-LH1, and the peripheral complex, LH2. The basic building block of LH2 is a protein heterodimer, which accommodates three BChl *a* pigments and one carotenoid molecule. For the species *Rhodopseudomonas acidophila*, the LH2 complex consists of nine copies of these heterodimers, which are arranged in a ring-like structure.[4] The BChl *a* molecules are arranged in two pigment pools, labeled B800 and B850, according to their room-temperature absorption maxima in the near-infrared. The B800 assembly comprises nine well-separated BChl *a* molecules, which have the planes of their bacteriochlorin rings aligned nearly perpendicular to the symmetry axis of the LH2 ring, whereas the B850 assembly comprises 18 BChl *a* molecules in close contact oriented with the plane of their bacteriochlorin rings parallel to the symmetry axis.

In the photosynthetic membrane, the RC-LH1 complexes are surrounded by the LH2 complexes and light-energy, absorbed by LH2, is transferred via LH1 to the RC.[5] Energy transfer within the LH2 complex occurs from B800 to the B850 in less than 1 ps.[6] Once the energy arrives in B850, it equilibrates within the B850 manifold an order of magnitude faster.[7,8] The transfer of energy from LH2 to LH1 and subsequently to the reaction center occurs in vivo within 3 ps[9] and 25−40 ps,[10,11] respectively, i.e. very fast compared to the decay of the B850 excited singlet state (^{1}B850*) within an isolated LH2, which process has a lifetime of about 1.1 ns.[12,13] Alternatively, the ^{1}B850* state can decay by intersystem crossing with a time constant on the order of 10 ns to a B850 triplet state (^{3}B850*) that is quenched by triplet−triplet energy transfer to an adjacent carotenoid.[14,15] The time constant for this process is also about 10 ns and the lifetime of the excited triplet state of the carotenoid (^{3}Car*) is about 7 μs.[16] These figures illustrate the well-known fact that under high illumination conditions the carotenoid acts as photoprotector, preventing the

Received: March 12, 2011
Revised: May 11, 2011
Published: June 07, 2011

formation of highly reactive singlet oxygen from a reaction between ^{3}B850* and $^3O_2$.[17] It appears that, in vivo, the whole structure is highly optimized for capturing light energy under various illumination conditions and funnelling it to the RC. The supramolecular architecture of these complexes in intact photosynthetic membranes, which is housed in chromatophores corresponding to extensions of the cytoplasmic membrane, has been imaged using atomic force microscopy (AFM).[18−21]

The character of the electronically excited states of the light-harvesting complexes from purple bacteria has been explored by countless groups exploiting time-resolved spectroscopy,[5,7−12,16,22−27] spectrally selective spectroscopy,[28−34] single-molecule spectroscopy,[35−44] or theoretical approaches.[45−56] Together with the high-resolution structural data that became available for some of the antenna complexes during the last two decades,[4,57−64] this work has led to a deep understanding of the structure/function relationships in this system.

For early studies on arrays of antennae, isolated LH2 complexes were not available and the experiments were performed on chromatophores that were directly extracted from the cells of the bacteria. Next to a large amount of LH2 these contained also other pigment−protein complexes, in particular RC-LH1, that influenced the kinetics of the electronically excited states. Further complications arose from the use of excitation pulses longer than 10 ns and/or repetition rates higher than 100 kHz, because this leads to the accumulation of long-lived triplet states.[65] As a consequence of this, the probability increases that a LH2 complex still carries an excited triplet state when the next 'flash' excites it again to the ^{1}B850* state. The interaction of these two electronic excitations on the same LH2 complex leads to singlet−triplet annihilation.[65] This results in a radiationless depletion of the ^{1}B850* state that shows up as a reduction of the fluorescence yield of this state. The probability for this process increases in chromatophores because of ^{1}B850* excitation energy transfer between the antenna complexes.[66] If the lifetime of the ^{1}B850* state is about 1 ns and the LH2 → LH2 energy transfer time is about 10 ps, it follows that in an array of LH2 complexes the excitation can travel within a region of a radius of about 10 antenna complexes and experiences a finite probability of encountering an LH2 complex that still carries an (immobile) ^{3}Car* excitation. The phenomenon of fluorescence quenching due to annihilation has now been known for more than 3 decades.[65] Experiments have mainly been conducted on chromatophores, containing several different pigment protein complexes, such as LH2, LH1, and RC. Although the microscopic structure of these complexes was unknown at that time, it was possible to draw conclusions about the supramolecular organization within the membrane due to the diffusion behavior of the B850 excitons. An overview of these findings can be found in refs 66−69 or ref 70 as a review.

It is still difficult to follow and therefore to understand the energy transfer reactions within arrays of a single type of antenna complex.[71] Such arrays have now been detected in vivo in membranes. It is possible to reconstitute LH2 complexes into phospholipid model membranes, providing a homoarray of identical antenna complexes. This study presents the first step toward investigating energy transfer reactions within such arrays of identical antenna complexes. The aim of the present work is to find out more about the performance of an array of natural LH2 complexes as a function of the excitation conditions. This study comprises experiments in combination with dynamic Monte Carlo (DMC) simulations. Since an isolated LH2 complex is already a complicated multichromophoric system, the results will be presented in two consecutive papers in the following referred to as parts I (this work) and II.[81] The current publication (part I) deals with isolated LH2 complexes in detergent solution. This allows the investigation of the singlet−triplet annihilation process on an isolated LH2 without any influence of LH2 → LH2 energy transfer. From this study, we obtain a simple four-state model with rate constants for the photophysical processes within an isolated LH2 ring, which forms the basic building block for the analysis of the further work. In part II,[81] we will present the results on arrays of reconstituted LH2 complexes. The information gained will be useful for understanding how the architecture of the light-harvesting apparatus in photosynthesis affects light-harvesting performance as well as for future applications of using such biological complexes in solar energy applications.

MATERIALS AND METHODS

Sample Preparation. The LH2 complexes from the species *R. acidophila* (strain 10050) were isolated and purified as described previously.[72] After purification, the LH2 complexes were transferred to a buffer containing 50 mM Glygly (Glycyl-Glycin, Roth, Karlsruhe, Germany) at pH 8 and 1% β-OG (octyl-β-D-glucopyranoside, Fluka, St Gallen, Switzerland) and stored in small aliquots at −80 °C until used.

Optical Setup. For the time-resolved experiments, the samples were excited at 800 nm with a pulsed titanium:sapphire laser (Tsunami, Spectra Physics) that was pumped with a frequency-doubled Nd:YVO4 laser (Millennia Xs, Spectra Physics). The pulse duration was about 2 ps, corresponding to a spectral bandwidth of 0.3 nm (3 cm^{-1}). The repetition rate of the excitation pulses was 81 MHz and could be decreased with a pulse picker unit (3980, Spectra Physics) to 8, 2, and 0.05 MHz, respectively.

In order to prevent irreversible photo bleaching, the sample was spun around with a frequency of 50 Hz in a home-built rotation cell. The fluorescence from the sample was collected at right-angle with respect to the direction of the excitation. The signal was spectrally resolved using an imaging spectrograph (250 IS, Bruker), providing a spectral resolution of 3 nm in the spectral range from 820 to 980 nm. The detector was a streak camera system (C5680, Hamamatsu Photonics) in combination with a CCD camera (Orca-ER C4752, Hamamatsu Photonics). In all these experiments, the streak camera system was operated in the time range of 5 ns, in single-sweep mode, providing an instrument response time of 50 ps (fwhm). For the fluorescence decays, the photon fluence per pulse incident onto the sample was adjusted to 3.3×10^{12}, 6.5×10^{12}, 13×10^{12}, and 26×10^{12} photons per pulse per cm^2. Conversions of these photon fluences per pulse to continuous illumination conditions are given in the Supporting Information.

The integrity of the LH2 samples was checked with an UV−vis absorption spectrometer (Perkin-Elmer, data not shown) before and after each streak experiment. No significant bleaching or irreversible sample damage could be detected under any of the excitation conditions used.

RESULTS

In order to study the influence of long-lived states on the decay kinetics of the LH2 complexes, time-resolved experiments were carried out as a function of the photon fluence, defined as number of photons per pulse and per area, and as a function of the laser repetition rate. The room-temperature emission spectrum of

LH2 was recorded upon repetitive excitation at 800 nm at rates of 81 MHz, 8 and 2 MHz, respectively. For each repetition rate, four spectra were registered as a function of the photon fluence, which was adjusted to 26×10^{12}, 13×10^{12}, 6.5×10^{12}, and 3.3×10^{12} photons/(pulse·cm^2). At a repetition of 50 kHz, the emission was only detectable for the two highest fluences. The resulting 14 emission spectra are shown in Figure 1.

Spectra that were recorded with the same repetition rate are shown as a group of four spectra (two for 50 kHz), each representing a different photon fluence. For better comparison, the spectra have been normalized and are offset with respect to each other by 0.1 within each group and 0.3 between the groups of spectra. All spectra feature a broad emission band centered at 865 nm with a width (fwhm) of 30 nm. A variation of the peak position and width of the spectra as a function of the excitation parameters was not observed. Since the streak system allows the detection of spectrally resolved fluorescence decays, we could verify that the decay kinetics did not depend on the emission wavelength. This justifies the assumption of being able to integrate the whole emission band in our further data analysis presented below.

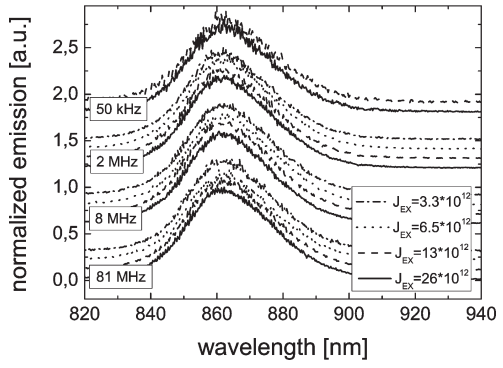

Figure 1. Normalized fluorescence emission spectra as a function of excitation fluence J_{EX} and pulse repetition rate. The four groups of spectra correspond from top to bottom to repetition rates of 50 kHz and 2, 8, and 81 MHz, respectively. Within each group the spectra correspond from top to bottom to fluences of 3.3×10^{12} (dash-dotted line), 6.5×10^{12} (dotted line), 13×10^{12} (dashed line), and 26×10^{12} (full line), given in photons/(pulse·cm^2), respectively. For clarity, the spectra have been offset by 0.1 within each group and by 0.3 between the groups.

The fluorescence decay of the LH2 emission is shown in Figure 2A for a repetition rate of 81 MHz as a function of the fluence. All transients are compatible with monoexponentials and the decay time decreases monotonically from 1080 ps for a fluence of 3.3×10^{12} photons/(pulse·cm^2) to 940 ps at 26×10^{12} photons/(pulse·cm^2). An example for the influence of the repetition rate on the fluorescence decay is shown in Figure 2B. For these experiments, the sample is excited with 26×10^{12} photons/(pulse·cm^2). Again all transients are monoexponentials, and only for the highest repetition rate, i.e. 81 MHz, can a significant reduction of the fluorescence lifetime from about 1100 to 940 ps be observed. The findings of similar experiments at the other fluences and repetition rates are summarized in Figure 3.

Only at the highest repetition rate of 81 MHz, there is a significant decrease of the fluorescence decay time as the fluence is increased. For all other repetition rates, 8 MHz, 2 MHz, and 50 kHz, respectively, the fluorescence decay time does not vary within experimental accuracy as a function of the fluence.

(Monte Carlo) Simulations. *The Model.* We will start this discussion by introducing the model on which we based the DMC simulations to explain our experimental data. Since a LH2 complex is a multichromophoric system consisting of 27 BChl a molecules and 9 carotenoids, featuring a rich photophysics

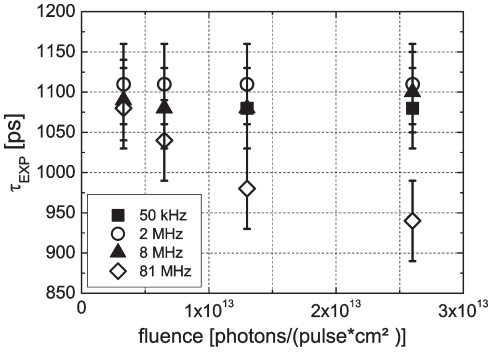

Figure 3. Decay times from monoexponential fits to the data for repetition rates of 50 kHz (circles), 2 MHz (squares), 8 MHz (triangles), and 81 MHz (diamonds), respectively, as a function of the excitation fluence.

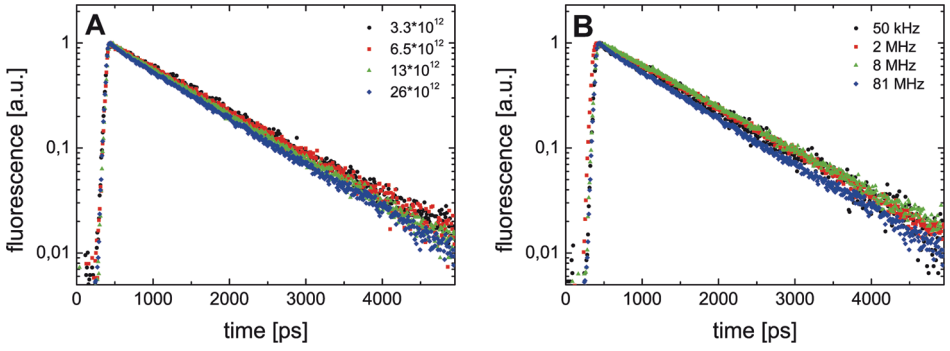

Figure 2. (A) Normalized fluorescence decays of isolated LH2 complexes in detergent solution for a repetition rate of 81 MHz as a function of fluence, which is given in photons/(pulse·cm^2): 3.3×10^{12} (black dots), 6.5×10^{12} (red squares), 13×10^{12} (green triangles), and 26×10^{12} (blue diamonds), respectively. (B) Normalized fluorescence decays of isolated LH2 complexes in detergent solution for a fluence of 26×10^{12} photons/(pulse·cm^2) as a function of the repetition rate: 50 kHz (black dots), 2 MHz (red squares), 8 MHz (green triangles), and 81 MHz (blue diamonds), respectively. The time resolution was 50 ps for all experiments.

dx.doi.org/10.1021/jp202353c |J. Phys. Chem. B 2011, 115, 8813–8820

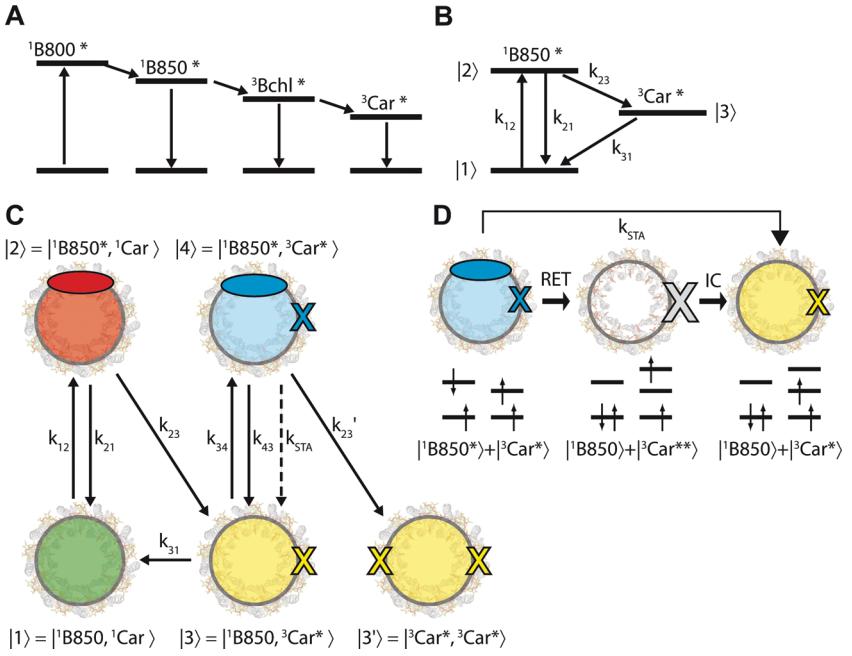

Figure 4. (A) Simplified energy level scheme for an isolated LH2 complex. (B) Further reduced energy level scheme for an isolated LH2 complex. (C) Pictorial representation of the transitions between the electronic states of an isolated LH2 complex taking singlet−triplet annihilation into account. (D) Simplified representation of singlet−triplet annihilation adapted from ref 75. The upper part corresponds to a pictorial representation; the lower part corresponds to a description in terms of one-electron molecular orbitals. For more details, see text.

including energy transfer processes and excitonic interactions between the chromophores that give rise to several types of quenching mechanisms, which cover time scales from some femtoseconds to microseconds, it is clear that an "exact" description of the full system on all time scales is out of reach. Therefore, our model carries several approximations and simplifications that are detailed below.

First, it is important to note that in our samples the β-OG concentration of 1% (w/w) corresponds to about 34 mM, which is well above the critical micellar concentration of 25 mM at 25 °C for this detergent. Using average LH2 concentrations in the order of μM, it is known that under these conditions aggregation of detergent micelles is avoided.[73] Therefore, in the following, the LH2 complexes were treated as isolated, noninteracting antenna complexes and intercomplex energy transfer was neglected. Further under high-illumination conditions, it becomes possible to create two excited ^{1}B850* states in the same LH2 complex, giving rise to singlet−singlet annihilation.[25] In ref 74, this phenomenon has been studied systematically as a function of the excitation intensity with LH2 complexes from *Rb. sphaeroides*. The authors of ref 74 found (i) that singlet−singlet annihilation occurs on a subpicosecond time scale and (ii) that fluences above 3×10^{14} photons/(pulse·cm^2) are required to have more than one singlet state on an individual LH2 complex. In the current study, the maximum fluence was 2.6×10^{13} photons/(pulse·cm^2), i.e., one order of magnitude lower than this value. Hence we exclude singlet−singlet annihilation for the individual, detergent solubilized samples (this will change in part II,[81] when we will discuss the presence of intercomplex energy transfer due to arrays of LH2 complexes[67]). Moreover, our time resolution does not allow the resolution of this process.

These considerations bring us as a starting point to the energy level scheme shown in Figure 4A, where the ^{1}B800*, ^{1}B850* etc. states are approximated as single levels. In our experiments, we neither resolve the ^{1}B800* → ^{1}B850* energy transfer nor the equilibration of the excitation within the B850 manifold. Also the quenching process of the ^{3}B850* triplet state by the carotenoid occurs with a time constant of 10 ns, which is very fast with respect to the direct decay of the ^{3}B850* triplet state to the ground state for which a time constant of 7 μs has been reported.[16] Led by these considerations, we further reduce the energy level scheme of an individual LH2 complex to an effective three-level system as shown in Figure 4B. Transitions between these states occur with rates k_{ij}, $i,j = 1, 2, 3$. However, we have to take into account singlet−triplet annihilation processes, which cannot be illustrated appropriately in this energy level scheme. Therefore, we have introduced a pictorial representation of the electronic states of a single LH2 complex in Figure 4C. This scheme has been proven to be very useful for the simulation of the excitation annihilation processes in the arrays of LH2 complexes (presented in part II[81]). A LH2 ring that is in the electronic ground state is represented by a circle. For brevity, we denote this state by $|1\rangle = |^1\text{B850}, {}^1\text{Car}\rangle$ (Figure 4C, green). A LH2 ring that carries a ^{1}B850* state is visualized as a circle with an ellipse and will be referred to as $|2\rangle = |^1\text{B850}^*, {}^1\text{Car}\rangle$ (Figure 4C, red). In the reduced energy level scheme the triplet state is located on one of the carotenoids. This state is represented by a circle with a cross and will be referred to as $|3\rangle = |^1\text{B850}, {}^3\text{Car}^*\rangle$ (Figure 4C, yellow). Singlet−triplet annihilation becomes possible if a LH2 ring that still carries a triplet state (cross) gets excited again to the ^{1}B850* state (ellipse), rate k_{34}. This situation is depicted by a circle with both a cross and an ellipse and will be referred to as $|4\rangle = |^1\text{B850}^*, {}^3\text{Car}^*\rangle$ (Figure 4C, blue). In addition to the radiative decay of the singlet excitation, rate k_{43}, state $|4\rangle$ can decay back to state $|3\rangle$ with a rate k_{STA} by singlet−triplet annihilation, as shown in more detail in Figure 4D according to a model introduced by Hofkens and de Schrijver et al. for multichromophoric systems.[75] In terms of one-electron molecular

orbitals, state $|4\rangle$ corresponds to a configuration as shown at the bottom on the left-hand side of Figure 4D. By resonance energy transfer (RET), the electron in the upper orbital on the carotenoid can be promoted to an even higher lying orbital at the expense of the electron in the upper orbital on the B850, which is moved simultaneously to the lower orbital. In terms of electronic states, this configuration corresponds to a higher excited triplet state on the carotenoid (^{3}Car**) indicated by the big cross. It is worth noting that this process can be very fast because the total spin is conserved. By internal conversion (IC), this state can relax nonradiatively to the lowest excited triplet state $|3\rangle$ on the carotenoid, right-hand side of Figure 4D. Hence, singlet−triplet annihilation corresponds to two consecutive steps, RET and IC, and the rate constant for this process is given by $k_{STA}^{-1} = k_{RET}^{-1} + k_{IC}^{-1}$. Finally, since LH2 is a multichromophoric system, it is also possible that a LH2 ring that is in state $|4\rangle$ decays with a rate k'_{23} to a state $|3'\rangle = |^3\text{Car}^*, {}^3\text{Car}^*\rangle$ having two triplet states on different carotenoids and giving rise to triplet−triplet annihilation.[14] Since it is known from ESR experiments that the triplet states on the carotenoids are immobile,[16] and because triplet−triplet energy transfer is mediated by the short-range exchange interaction, we neglect triplet−triplet annihilation in our analysis as well as LH2 rings that carry two triplet excitations prior to the next excitation pulse. However, we do take into account the additional decay channels of state $|4\rangle$, which we summarize in the rate $k_q = k'_{23} + k_{STA}$.

This simple four-state model qualitatively explains our experimental observations. For a high repetition rate, the probability of finding a substantial amount of LH2 complexes in state $|3\rangle$ prior to the next excitation pulse is high. Hence, singlet−triplet annihilation processes, contributing to an accelerated depletion of the ^{1}B850* states, are highly probable. Increasing the fluence at high repetition rate leads to a growth of the population of the triplet state prior to the next excitation pulse and concomitantly to a larger relative contribution of the singlet−triplet annihilation to the decay of the ^{1}B850* state.

The DMC Algorithm. In order to test our model quantitatively, we performed numerical simulations of the fluorescence response as a function of the excitation parameters. In principle the kinetics of the systems could be modeled by solving a master equation. However, an analytical solution of a set of coupled rate equations becomes impossible due to the pulsed excitation. Under these conditions, the excitation rate is a function of time and it is only possible to estimate the populations of the various states by a separation of time scales.[76] Instead we employ a dynamic Monte Carlo algorithm[77−79] that is particularly useful to model repetitive pulsed excitation, because the serial execution of the Monte Carlo cycle refers to the successive excitation of the sample and the statistical average over a sufficient number of excitation cycles provides a fast numerical solution of the respective kinetic equations.

The excitation pulses are treated as δ-pulses, which is justified because the pulse duration of 2 ps is well below the experimental time resolution. The transitions between the states $|1\rangle$ to $|4\rangle$ are considered as incoherent quantum jumps, which allows the representation of the system by Poissonian statistics. Initially, the system is in the electronic ground state $|1\rangle$. By comparing a random number ρ_p, chosen from a uniform distribution between 0 and 1, with the excitation probability p_{12} (vide infra), it is decided whether the system is excited by the pulse ($\rho_p \leq p_{12}$) to state $|2\rangle$ or whether it remains in state $|1\rangle$ ($\rho_p > p_{12}$). (This procedure is applied also for an excitation from state $|3\rangle$ to $|4\rangle$ with the probability p_{34}.) In the case of an excitation, the DMC cycle runs as follows: State $|2\rangle$ acts as initial state $|i\rangle$. Then the value $K_i = \sum_{j=1}^{J} k_{ij}$ is calculated, where the sum runs over all J decay rates k_{ij} that are connected with the initial state $|i\rangle$. Next, two random numbers, ρ_1 and ρ_2, are chosen from a uniform distribution between 0 and 1. The first random number determines the time interval when the next quantum jump occurs from an exponential distribution according to $\Delta t = (1)/(K_i) \ln((1)/(\rho_1))$. The second random number determines which quantum jump occurs by the comparison of $(\sum_{j=1}^{m} k_{ij})/(K_i) \leq \rho_2 < (\sum_{j=m+1}^{J} k_{ij})/(K_i)$. Subsequently, state $|m\rangle$ becomes the initial state for the next cycle. These cycles are repeated until the time $1/k_{REP}$ is accumulated, where k_{REP} corresponds to the repetition rate of the laser. Then the next excitation cycle starts again with the determination of ρ_p. Each simulation covers 10^5 excitation cycles and runs in parallel on 61 four-level systems in order to speed up the calculation. The simulations provide the evolution of the populations of the states $|1\rangle$ to $|4\rangle$. In order to compare the results of the simulations with the experimentally determined fluorescence decays, all quantum jumps that correspond to the emission of a fluorescence photon, i.e. $|2\rangle \rightarrow |1\rangle$ and $|4\rangle \rightarrow |3\rangle$, are counted and the respective time increment is stored in computer memory. After finishing the excitation cycles, these increments are fed into a histogram (binning time 10 ps), which represents the simulated fluorescence transient. We note that the rates k_{21} and k_{43} are treated as purely radiative rates. This is justified because we compare only normalized fluorescence decays. Discriminating between radiative and nonradiative decays in the simulations would only reduce the emission yield by a constant factor without affecting the shape of the fluorescence transients.

Application of this algorithm requires the specification of the excitation probability and the rates k_{ij} and k_{STA} as input parameters. The excitation rate k_{12} for the $|2\rangle \leftarrow |1\rangle$ transition can be obtained from $k_{12} = I_{EX}\sigma_{800}$, with the absorption cross section at the excitation wavelength σ_{800} and the number of photons per area and time incident onto the sample I_{EX}. The cross section has been determined to $\sigma_{800} = 1.0 \times 10^{-14}$ cm^2 from the extinction at 850 nm and correction for the different absorption strengths in the B800 and B850 bands.[82] However, for pulsed excitation we have to determine the probability p_{12} of excitation of one LH2 complex during the excitation pulse. Under nonsaturating conditions of the optical transition this is given by $p_{12} = J_{EX}\sigma_{800}$, where J_{EX} denotes the fluence of photons per pulse and area. For example, at the highest fluence in our experiments we obtain a value of $p_{12} = 0.26$. The rates $k_{23} = 5 \times 10^7$ s^{-1} and $k_{31} = 1.4 \times 10^5$ s^{-1} were taken from the literature.[14,16] In order to keep the number of input parameters as small as possible, we assume that the absorption cross section at 800 nm of the LH2 complex that still carries a triplet state is unaltered with respect to an LH2 complex where all BChl and Car molecules are in the ground state, and vice versa for the decay of an excitation located on the B850 manifold. In other words, we set $k_{34} = k_{12}$ (or equivalently $p_{34} = p_{12}$) and $k_{43} = k_{21}$. Then, within the framework of the four-state model, the general fluorescence response of the sample is given by

$$I(t) = A_2 \exp(-(k_{21} + k_{23})t) + A_4 \exp(-(k_{21} + k_q)t) \quad (1)$$

where the A_n values denote the amplitudes associated with the states $|2\rangle$ and $|4\rangle$, respectively. The rate k_{21} can be determined from the decay of state $|2\rangle$ as long as singlet−triplet annihilation processes can be neglected, i.e., $A_4 \approx 0$. This limit is reasonably

well fulfilled for the experiments with a repetition rate of 50 kHz for which a decay time of 1080 ps was found for state $|2\rangle$. Hence $1/(1080\ \text{ps}) = k_{21} + k_{23}$, from which we deduce $k_{21} = 8.8 \times 10^8\ \text{s}^{-1}$. Finally, we have to specify the rate k_q which includes the singlet−triplet annihilation rate k_{STA}. Even for the highest fluences at the highest repetition rates, i.e., in the regime where singlet−triplet annihilation processes are effective, we do not observe a biexponential decay of the fluorescence. This indicates that in eq 1 the sum of the rates $(k_{21} + k_{23})$ on the one hand and $(k_{21} + k_q) = (k_{21} + k'_{23} + k_{STA})$ on the other hand are in the same order of magnitude preventing the resolution of two components in the transients. However, from that we can obtain a lower boundary for k_{STA}. For the extreme situation where all LH2 complexes reside in state $|3\rangle$ prior to the next excitation pulse, i.e., $A_2 \approx 0$ and $A_4 \approx 1$, the fluorescence decays with the rate constant $k_{21} + k'_{23} + k_{STA}$. The closest approximation to this situation corresponds to the experiments at the highest fluences and the highest repetition rates for which we found a decay time of 940 ps. From this value, we can deduce $k'_{23} + k_{STA} \approx 1.8 \times 10^8\ \text{s}^{-1}$. Approximating $k'_{23} = k_{23}$ for the rate of intersystem crossing into the triplet state of another Car molecule we find $k_{STA} = 1.3 \times 10^8\ \text{s}^{-1}$ as an lower boundary for the effective singlet−triplet annihilation rate. With these considerations, we arrive at a full set of input parameters for the DMC simulations which is summarized in Table 1.

Results of the DMC Simulations. Figure 5A shows the simulated fluorescence decays at a repetition rate of 81 MHz as a function of the fluence. All transients are in agreement with monoexponential decays and the simulated decay times τ_{sim} decrease monotonically from 1000 ps at a fluence of 3.3×10^{12} photons/(pulse·cm^2) to 960 ps at a fluence of 26×10^{12} photons/(pulse·cm^2).

Table 1. Input Parameters for the DMC Simulation

transfer rates	values [s^{-1}]	reference
$k_{12} \rightarrow p_{12}$	$J_{EX}\sigma_{800}$	
k_{21}	8.8×10^8	this work
$k_{23} = k'_{23}$	5×10^7	14
k_{31}	1.4×10^5	16
$k_{34} \rightarrow p_{34}$	$= p_{12} = J_{EX}\sigma_{800}$	
k_{43}	$= k_{21} = 8.8 \times 10^8$	
$k_q = k'_{23} + k_{STA}$	1.8×10^8	this work

Together with the results of the simulations for the other repetition rates these data are compared in Table 2 with the decay times τ_{exp} that have been determined experimentally. The simulated and experimentally obtained decay times, in the main, agree with each other within the limits of the experimental accuracy. Only four parameter combinations, i.e., 2 MHz and 8 MHz at the highest fluence, and 81 MHz at the two lowest fluences, show discrepancies between τ_{sim} and τ_{exp} amounting to 60−80 ps, which is still less than 10% of the absolute value. The simulations for 81 MHz, however, do reproduce correctly the decrease of the fluorescence lifetimes with increasing fluence. A slight decrease of the lifetime for increasing fluence is also predicted at 2 MHz and at 8 MHz but below the experimental time resolution. For 50 kHz, τ_{sim} shows to within 10 ps no variation as a function of the fluence, in agreement with the experimental observations.

Since the numerical simulations provide a complete solution of the temporal development of the four-state model, we have also access to the evolution of the population of the triplet state. At the highest repetition rate and with the four fluences applied, we show in Figure 5B the remaining relative population in the triplet state prior to the next excitation pulse as a function of the number of excitation cycles. For all fluences, the relative number of LH2 complexes that still carry a triplet state prior to the next excitation pulse shows a steep increase and asymptotically approaches a constant value, termed $\langle n_3 \rangle$ in the following. The value of $\langle n_3 \rangle$ is larger the larger the fluence applied, and varies from about 50% for the lowest fluence to 90% for the highest fluence. For the other repetition rates, the values of $\langle n_3 \rangle$ are also given in Table 2. In agreement with the qualitative considerations given above, $\langle n_3 \rangle$ is negligible for a repetition rate of 50 kHz and a significant triplet population is accumulated only with the repetition rates that are significantly larger than the inverse of the triplet lifetime. For our estimate of the lower boundary of k_{STA}, we have made the assumption that the triplet population at the highest fluence and the highest repetition rate is 100%. The simulations indicate that this assumption is nearly fulfilled, which allows the conclusion that the lower boundary of $k_{STA} = 1.3 \times 10^8\ \text{s}^{-1}$ is very close to the actual value of the rate constant for singlet−triplet annihilation.

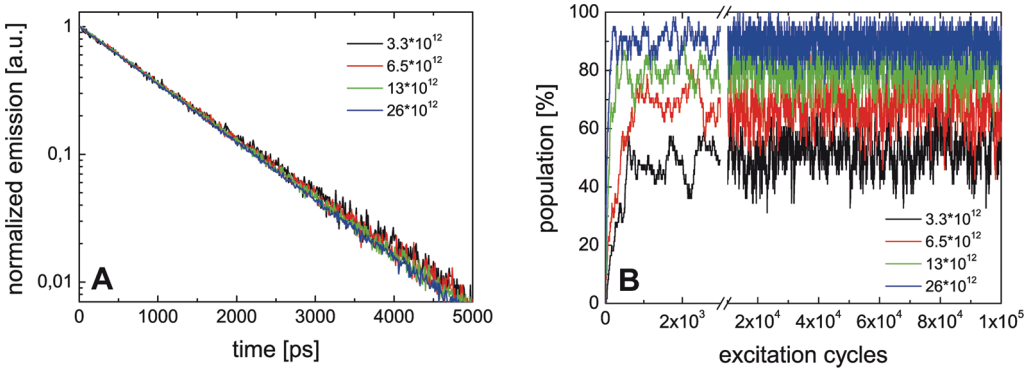

Figure 5. (A) Fluorescence decay curves from DMC simulations for the four-state model shown in Figure 4.C for a repetition rate of 81 MHz as a function of excitation fluence: 3.3×10^{12} (black), 6.5×10^{12} (red), 13×10^{12} (green), and 26×10^{12} (blue), given in photons/(pulse·cm^2), respectively. (B) Development of the population of the triplet state as a function of the number of excitation cycles for a repetition rate of 81 MHz and for fluences of 3.3×10^{12} (black), 6.5×10^{12} (red), 13×10^{12} (green), and 26×10^{12} (blue) photons/(pulse·cm^2), respectively. The first 2500 excitation cycles are shown on an expanded scale to better show the transient growth of the population in the triplet state before it levels off to an average value $\langle n_3 \rangle$.

dx.doi.org/10.1021/jp202353c |J. Phys. Chem. B 2011, 115, 8813–8820

Table 2. Comparison of the Experimental Decay Times τ_{EXP} with the Simulated Decay Times τ_{SIM} for the Various Repetition Rates and Fluences

	k_{REP} = 81 MHz			k_{REP} = 8 MHz			k_{REP} = 2 MHz			k_{REP} = 50 kHz		
J_{EX} [photons/ (pulse·cm^2)]	τ_{EXP} [ps]	τ_{SIM} [ps]	$\langle n_3 \rangle^a$ [%]	τ_{EXP} [ps]	τ_{SIM} [ps]	$\langle n_3 \rangle^a$ [%]	τ_{EXP} [ps]	τ_{SIM} [ps]	$\langle n_3 \rangle^a$ [%]	τ_{EXP} [ps]	τ_{SIM} [ps]	$\langle n_3 \rangle^a$ [%]
3.3×10^{12}	1080	1000	52	1090	1070	10	1110	1070	3		1080	0
6.5×10^{12}	1040	980	67	1080	1060	16	1110	1070	5		1070	0
13×10^{12}	980	970	80	1080	1040	30	1110	1060	8	1080	1070	0
26×10^{12}	940	960	90	1100	1020	46	1110	1050	16	1080	1080	0

[a] $\langle n_3 \rangle$ is the relative asymptotic triplet population as a function of the excitation parameters.

However, the simulations also reveal a discrepancy between the simulated and the experimental lifetimes. On the basis of the line of reasoning given above, one would expect that a relative triplet population of about 50% (81 MHz, lowest fluence) would lead to a reduction of the fluorescence lifetime with respect to a situation of 0% triplet population (50 kHz). While this trend is clearly reproduced by the simulations, i.e., 1000 vs 1080 ps, the experimentally observed lifetime is 1080 ps for both situations. Apparently, the four-state model slightly overestimates the remaining relative populations in the triplet state, which might reflect the action of a process that quenches the triplet population and which has not been considered in the analysis. Since for low triplet populations, the results of the simulations are in good agreement with the experiments, this process should be more effective if the triplet state is already significantly populated. Hence, a very likely candidate for such a process is triplet−triplet annihilation. We have neglected this process due to the low mobility of the triplet states and the short-range interaction between the triplet states on different carotenoids. However, at high excitation rates the probability increases that (i) several carotenoid molecules within one LH2 complex reside in the triplet state prior to the next excitation pulse or (ii) that the same carotenoid molecule within one LH2 complex will receive two excitations to the triplet state. For both situations, the chance for subsequent triplet−triplet annihilation increases tremendously leading to a stronger reduction of the triplet population than that predicted in our model.

CONCLUSIONS

We have presented a description for the photophysical processes in the multichromophoric LH2 complex from the photosynthetic purple bacterium *Rps. acidophila* in terms of a four-state model. Short comings of this model concern processes on time scales faster than ps, which are not covered here, and a slight overestimation of the population of the triplet state. Yet, given the remarkably simple four-state model, a good description of the photophysical processes on the picosecond time scale within an isolated LH2 complex is achieved, without the need for any free parameters. We now move on to the more challenging situations of consideration of LH2 homoarrays in part II.[81]

ASSOCIATED CONTENT

Supporting Information. Conversions of the fluence at different repetition rates to einsteins and to an equivalent continuous (CW) excitation intensity. This material is available free of charge via the Internet at http://pubs.acs.org.

AUTHOR INFORMATION

Corresponding Author

*Telephone: +49 921 55 4000. Fax: +49 921 55 4002. E-mail: juergen.koehler@uni-bayreuth.de.

ACKNOWLEDGMENT

Financial support from the Bavarian Science Foundation, the German Science Foundation (DFG; GRK 1640; DFG−UL 174/7-1), the Biotechnology and Biological Sciences Research Council (BBSRC) and the Engineering and Physical Sciences Research Council (EPSRC) is gratefully acknowledged. T.J.P. thanks F. Spreitler and E. Bombarda for fruitful discussions.

REFERENCES

(1) Blankenship, R. E. *Molecular Mechanisms of Photosynthesis*: Blackwell Science: Oxford, U.K., 2002.
(2) Hu, X.; Ritz, T.; Damjanovic, A.; Autenrieth, F.; Schulten, K. *Q. Rev. Biophys.* **2002**, *35*, 1–62.
(3) Cogdell, R. J.; Gall, A.; Köhler, J. *Q. Rev. Biophys.* **2006**, *39*, 227–324.
(4) McDermott, G.; Prince, S. M.; Freer, A. A.; Hawthornthwaite-Lawless, A. M.; Papiz, M. Z.; Cogdell, R. J.; Isaacs, N. W. *Nature* **1995**, *374*, 517–521.
(5) Sundström, V.; Pullerits, T.; van Grondelle, R. *J. Phys. Chem. B* **1999**, *103*, 2327–2346.
(6) Shreve, A. P.; Trautman, J. K.; Frank, H. A.; Owens, T. G.; Albrecht, A. C. *Biochim. Biophys. Acta* **1991**, *1058*, 280–288.
(7) Jimenez, R.; Dikshit, S. N.; Bradford, S. E.; Fleming, G. R. *J. Phys. Chem.* **1996**, *100*, 6825–6834.
(8) Kennis, J. T. M.; Streltsov, A. M.; Vulto, S. I. E.; Aartsma, T. J.; Nozawa, T.; Amesz, J. *J. Phys. Chem. B* **1997**, *101*, 7827–7834.
(9) Hess, S.; Chachisvilis, M.; Timpmann, K.; Jones, M.; Fowler, G.; Hunter, C.; Sundström, V. *Proc. Natl. Acad. Sci. U.S.A.* **1995**, *92*, 12333–12337.
(10) Bergström, H.; van Grondelle, R.; Sundström, V. *FEBS Lett.* **1989**, *250*, 503–508.
(11) Visscher, K. J.; Bergström, H.; Sundström, V.; Hunter, C. N.; Grondelle, R. *Photosynth. Res.* **1989**, *22*, 211–217.
(12) Monshouwer, R.; Abrahamson, M.; van Mourik, F.; van Grondelle, R. *J. Phys. Chem. B* **1997**, *101*, 7241–7248.
(13) Pflock, T.; Dezi, M.; Venturoli, G.; Cogdell, R.; Köhler, J.; Oellerich, S. *Photosynth. Res.* **2008**, *95*, 291–298.
(14) Monger, T. G.; Cogdell, R. J.; Parson, W. W. *Biochim. Biophys. Acta* **1976**, *449*, 136–153.
(15) Cogdell, R. J.; Hipkins, M. F.; MacDonald, W.; Truscott, T. G. *Biochim. Biophys. Acta* **1981**, *634*, 191–202.
(16) Bittl, R.; Schlodder, E.; Geisenheimer, I.; Lubitz, W.; Cogdell, R. J. *J. Phys. Chem. B* **2001**, *105*, 5525–5535.
(17) Cogdell, R. J.; Frank, H. A. *Biochim. Biophys. Acta* **1987**, *895*, 63–79.

(18) Bahatyrova, S.; Frese, R. N.; Siebert, C. A.; Olsen, J. D.; van der Werf, K. O.; van Grondelle, R.; Niederman, R. A.; Bullough, P. A.; Otto, C.; Hunter, C. N. *Nature* **2004**, *430*, 1058–1062.
(19) Scheuring, S.; Sturgis, J. N.; Prima, V.; Bernadac, A.; Levy, D.; Rigaud, J. L. *Proc. Natl. Acad. Sci. U.S.A.* **2004**, *101*, 11293–11297.
(20) Goncalves, R. P.; Bernadac, A.; Sturgis, J. N.; Scheuring, S. *J. Struct. Biol.* **2005**, *152*, 221–228.
(21) Scheuring, S.; Goncalves, R. P.; Prima, V.; Sturgis, J. N. *J. Mol. Biol.* **2006**, *358*, 83–96.
(22) Freiberg, A.; Godik, V. I.; Pullerits, T.; Timpman, K. *Biochim. Biophys. Acta* **1989**, *973*, 93–104.
(23) Timpmann, K.; Freiberg, A.; Godik, V. I. *Chem. Phys. Lett.* **1991**, *182*, 617–622.
(24) Blankenship, R. E.; Madigan, M. T.; Bauer, C. E. *Anoxygenic Photosynthetic Bacteria*; Kluwer Academic Publishers: Dordrecht, The Netherlands, 1995; pp 350−372.
(25) Ma, Y.-Z.; Gogdell, R. J.; Gillbro, T. *J. Phys. Chem. B* **1997**, *101*, 1087–1095.
(26) Zinth, W.; Wachtveitl, J. *ChemPhysChem* **2005**, *6*, 871–880.
(27) Engel, G. S.; Calhoun, T. R.; Read, E. L.; Ahn, T. K.; Mancal, T.; Cheng, Y. C.; Blankenship, R. E.; Fleming, G. R. *Nature* **2007**, *446*, 782–786.
(28) Matsuzaki, S.; Zazubovich, V.; Fraser, N. J.; Cogdell, R. J.; Small, G. J. *J. Phys. Chem. B* **2001**, *105*, 7049–7056.
(29) Rätsep, M.; Wu, H.-M.; Hayes, J. M.; Blankenship, R. E.; Cogdell, R. J.; Small, G. J. *J. Phys. Chem. B* **1998**, *102*, 4035–4044.
(30) Wu, H.-M.; Rätsep, M.; Lee, I.-J.; Cogdell, R. J.; Small, G. J. *J. Phys. Chem. B* **1997**, *101*, 7654–7663.
(31) de Caro, C.; Visschers, R. W.; van Grondelle, R.; Völker, S. *J. Phys. Chem.* **1994**, *98*, 10584–10590.
(32) Purchase, R.; Völker, S. *Photosynth. Res.* **2009**, *101*, 245–266.
(33) Rätsep, M.; Hunter, C. N.; Olsen, J. D.; Freiberg, A. *Photosynth. Res.* **2005**, *86*, 37–48.
(34) Rätsep, M.; Freiberg, A. *Chem. Phys. Lett.* **2003**, *377*, 371–376.
(35) Bopp, M. A.; Sytnik, A.; Howard, T. D.; Cogdell, R. J.; Hochstrasser, R. M. *Proc. Natl. Acad. Sci. U.S.A.* **1999**, *96*, 11271–11276.
(36) Tietz, C.; Cheklov, O.; Dräbenstedt, A.; Schuster, J.; Wrachtrup, J. *J. Phys. Chem. B* **1999**, *103*, 6328–6333.
(37) Rutkauskas, D.; Novoderezkhin, R.; Cogdell, R. J.; van Grondelle, R. *Biochemistry* **2004**, *43*, 4431–4438.
(38) Ketelaars, M.; Hofmann, C.; Köhler, J.; Howard, T. D.; Cogdell, R. J.; Schmidt, J.; Aartsma, T. J. *Biophys. J.* **2002**, *83*, 1701–1715.
(39) Hofmann, C.; Francia, F.; Venturoli, G.; Oesterhelt, D.; Köhler, J. *FEBS Lett.* **2003**, *546*, 345–348.
(40) Hofmann, C.; Aartsma, T. J.; Köhler, J. *Chem. Phys. Lett.* **2004**, *395*, 373–378.
(41) van Oijen, A. M.; Ketelaars, M.; Köhler, J.; Aartsma, T. J.; Schmidt, J. *Science* **1999**, *285*, 400–402.
(42) Cogdell, R. J.; Köhler, J. *Biochem. J.* **2009**, *422*, 193–205.
(43) Hofmann, C.; Michel, H.; van Heel, M.; Köhler, J. *Phys. Rev. Lett.* **2005**, *94*, 195501.
(44) Brotosudarmo, T. H. P.; Kunz, R.; Böhm, P.; Gardiner, A. T.; Moulisová, V.; Cogdell, R. J.; Köhler, J. *Biophys. J.* **2009**, *97*, 1491–1500.
(45) Alden, R. G.; Johnson, E.; Nagarajan, V.; Parson, W. W.; Law, C. J.; Cogdell, R. J. *J. Phys. Chem. B* **1997**, *101*, 4667–4680.
(46) Sauer, K.; Cogdell, R. J.; Prince, S. M.; Freer, A. A.; Isaacs, N. W.; Scheer, H. *Photochem. Photobiol.* **1996**, *64*, 564–576.
(47) Jang, S.; Silbey, R. J. *J. Chem. Phys.* **2003**, *118*, 9312–9323.
(48) Jang, S.; Silbey, R. J. *J. Chem. Phys.* **2003**, *118*, 9324–9336.
(49) Jang, S.; Dempster, S. E.; Silbey, R. J. *J. Phys. Chem. B* **2001**, *105*, 6655–6665.
(50) Dempster, S. E.; Jang, S.; Silbey, R. J. *J. Chem. Phys.* **2001**, *114*, 10015–10023.
(51) Beljonne, D.; Curutchet, C.; Scholes, G. D.; Silbey, R. J. *J. Phys. Chem. B* **2009**, *113*, 6583–6599.
(52) Mostovoy, M. V.; Knoester, J. *J. Phys. Chem. B* **2000**, *104*, 12355–12364.
(53) Didraga, C.; Knoester, J. *J. Chem. Phys.* **2002**, *275*, 307–318.
(54) Mukai, K.; Abe, S.; Sumi, H. *J. Phys. Chem. B* **1999**, *103*, 6096–6102.
(55) Krueger, B. P.; Scholes, G. D.; Fleming, G. R. *J. Phys. Chem. B* **1998**, *102*, 5378–5387.
(56) Cory, M. G.; Zerner, M. C.; Hu, X.; Schulten, K. *J. Phys. Chem. B* **1998**, *102*, 7640–7650.
(57) Karrasch, S.; Bullough, P. A.; Ghosh, R. *EMBO J.* **1995**, *14*, 631–638.
(58) Walz, T.; Jamieson, S. J.; Bowers, C. M.; Bullough, P. A.; Hunter, C. N. *J. Mol. Biol.* **1998**, *282*, 833–845.
(59) Koepke, J.; Hu, X.; Muenke, C.; Schulten, K.; Michel, H. *Structure* **1996**, *4*, 581–597.
(60) McLuskey, K.; Prince, S. M.; Cogdell, R. J.; Isaacs, N. W. *Biochemistry* **2001**, *40*, 8783–8789.
(61) Papiz, M. Z.; Prince, S. M.; Howard, T.; Cogdell, R. J.; Isaacs, N. W. *J. Mol. Biol.* **2003**, *326*, 1523–1538.
(62) Roszak, A. W.; Howard, T. D.; Southall, J.; Gardiner, A. T.; Law, C. J.; Isaacs, N. W.; Cogdell, R. J. *Science* **2003**, *302*, 1969–1971.
(63) Siebert, C. A.; Qian, P.; Fotiadis, D.; Engel, A.; Hunter, C. N.; Bullough, P. A. *EMBO J.* **2004**, *23*, 690–700.
(64) Qian, P.; Neil Hunter, C.; Bullough, P. A. *J. Mol. Biol.* **2005**, *349*, 948–960.
(65) Monger, T. G.; Parson, W. W. *Biochim. Biophys. Acta* **1977**, *460*, 393–407.
(66) Westerhuis, W. H. J.; Vos, M.; van Grondelle, R.; Amesz, J.; Niederman, R. A. *Biochim. Biophys. Acta* **1998**, *1366*, 317–329.
(67) Deinum, G.; Otte, S. C. M.; Gardiner, A. T.; Aartsma, T. J.; Cogdell, R. J.; Amesz, J. *Biochim. Biophys. Acta* **1991**, *1060*, 125–131.
(68) Law, C. J.; Cogdell, R. J.; Trissl, H.-W. *Photosynth. Res.* **1997**, *52*, 157–165.
(69) Trissl, H. W.; Law, C. J.; Cogdell, R. J. *Biochim. Biophys. Acta* **1999**, *1412*, 149–172.
(70) van Amerongen, H.; Valkunas, L.; van Grondelle, R. *Photosynthetic Excitons*; World Scientific: Singapore, 2000.
(71) Strümpfer, J.; Schulten, K. *J. Chem. Phys.* **2009**, *131*, 225101–9.
(72) Gardiner, A. T.; Cogdell, R. J.; Takaichi, S. *Photosynth. Res.* **1993**, *38*, 159–167.
(73) Cogdell, R. J.; Durant, I.; Valentine, J.; Lindsay, J. G.; Schmidt, K. *Biochim. Biophys. Acta* **1983**, *722*, 427–435.
(74) Trinkunas, G.; Herek, J. L.; Polívka, T.; Sundström, V.; Pullerits, T. *Phys. Rev. Lett.* **2001**, *86*, 4167.
(75) Hofkens, J.; Cotlet, M.; Vosch, T.; Tinnefeld, P.; Weston, K. D.; Ego, C.; Grimsdale, A.; Müllen, K.; Beljonne, D.; Bredas, J. L.; Jordens, S.; Schweitzer, G.; Sauer, M.; de Schryver, F. *Proc. Natl. Acad. Sci U.S.A.* **2003**, *100*, 13146–13151.
(76) Valkunas, L.; Liuolia, V.; Freiberg, A. *Photosynth. Res.* **1991**, *27*, 83–95.
(77) Gillespie, D. T. *J. Phys. Chem.* **1977**, *81*, 2340–2361.
(78) Fichthorn, K. A.; Weinberg, W. H. *J. Chem. Phys.* **1991**, *95*, 1090–1096.
(79) Till, M. S.; Essigke, T.; Becker, T.; Ullmann, G. M. *J. Phys. Chem. B* **2008**, *112*, 13401–13410.
(80) Clayton, R. K.; Clayton, B. J. *Proc. Natl. Acad. Sci. U.S.A.* **1981**, *78*, 5583–5587.
(81) Pflock, T.; Oellerich, S.; Krapf, L.; Southall, J.; Cogdell, R.; Ullmann, G. M.; Köhler, J. *J. Phys. Chem. B* **2011**10.1021/jp2023583.
(82) From the extinction of 184 L/(mol·cm) for one B850 BChl a molecule,[80] $\varepsilon_{B850} = 18 \cdot 184$ L/(mol·cm) = 3.3×10^3 L/(mol·cm) is obtained. Multiplication with the B800/B850 peak absorption ratio (here 0.78) yields $\varepsilon_{B800} = 2.6 \times 10^3$ L/(mol·cm). The absorption cross section is obtained by the usual conversion $\sigma_{800} = \ln 10 \times \varepsilon_{800}/N_A$, with N_A being Avogadro's number.